ELSEVIER

Polymer 44 (2003) 413–422

polymer

www.elsevier.com/locate/polymer

Effect of salt additive on the formation of microporous poly(vinylidene fluoride) membranes by phase inversion from $LiClO_4$/Water/DMF/PVDF system

Dar-Jong Lin, Cheng-Liang Chang, Fane-Ming Huang, Liao-Ping Cheng*

Department of Chemical Engineering, Tamkang University, Taipei 25137, Taiwan, ROC

Received 14 August 2002; received in revised form 17 September 2002; accepted 8 October 2002

Abstract

The effect of a salt additive, lithium perchlorate, on the morphology and crystal structure of PVDF membranes prepared by wet phase inversion process was studied. The gelation phase boundaries of the quaternary system, LiClO4/water/DMF/PVDF, were determined at 25 °C. It was found that the gelation lines shifted up progressively with increasing salt contents in this system. For a salt-free casting dope, the formed membrane exhibited a typical asymmetric structure characterized by the skin, parallel columnar macrovoids, and cellular pores. WAXD analysis indicated that PVDF crystallized into 'α' (type II) structure in this membrane. By contrast, when PVDF was precipitated from high salt-content dopes (e.g. ≥5 wt%), the macrovoids bent and extended towards the bottom region while the original cellular pores evolved into very large voids. The PVDF crystallites became 'β' form (type I) in these membranes. Thermal analysis (DSC) of all membranes showed dual melting peaks at low heating rates (≤5 °C/min), suggesting that the crystallites formed in the immersion–precipitation process were imperfect and they underwent re-crystallization during the heating process. Using low voltage SEM at high magnifications (e.g. 100 KX at 0.55 KV) on uncoated samples, the fine structures (10–20 nm) of the PVDF crystallites were observed. And at very high magnifications (225 KX at 0.59 KV), it was observed that the skin region of the membrane prepared from high salt-content dopes actually contained many nano-pores (e.g. 20 nm). This contributes to the high permeation rate and low solute rejection as revealed from the water-flux measurements.
© 2002 Elsevier Science Ltd. All rights reserved.

Keywords: Poly(vinylidene fluoride); Membrane; Crystallization

1. Introduction

Addition of inorganic salts in casting dope to prepare porous membranes by phase inversion method has been an effective practice to improve the permeability and/or selectivity of ultrafiltration membranes [1–5]. Bottino et al. [2] used lithium chloride doped casting solutions to prepare poly(vinylidene fluoride) membranes with higher porosity and better overall performance than that without adding salt in the dope. Kim et al. [3] observed the electroviscous behavior caused by adding zinc chloride in polysulfone/NMP solutions and interpreted this behavior in terms of interactions between salt and polymer. The formed membranes were reported to exhibit an increased rejection rate and a decreased molecular weight cut-off. Instead of using pure salt, Kraus et al. [4] applied salt mixtures in aromatic polyamide/dimethylacetamide solutions for membrane preparation. A stronger effect on the membrane structure and performance than single salt additive was reported. Recently, Wang et al. [5] used nonsolvent/LiCl mixture as an additive and produced PVDF hollow fibers with improved permeability and good mechanical strength. Salt additives were also used to prepare membranes for certain separation purposes; e.g. Lai et al. [6] prepared $(PMMA/CH_2Cl_2)/(DMF/CuCl_2{\cdot}2H_2O)$ complex membranes for separation of oxygen from nitrogen.

In a previous paper, a mechanism for the formation PVDF membrane by immersion–precipitation from water/DMF solution was described on the basis of phase behavior and mass transfer modeling [7]. In principle, the sequence of precipitation events (i.e. crystallization and/or liquid–liquid demixing), which can be manipulated by the dope and the bath conditions, dictated the ultimate

* Corresponding author. Tel.: +886-2-26215656x2614/2725; fax: +886-2-26209887.
E-mail address: lpcheng@mail.tku.edu.tw (L.P. Cheng).

0032-3861/03/$ - see front matter © 2002 Elsevier Science Ltd. All rights reserved.
PII: S0032-3861(02)00731-0

Table 1
Composition and viscosities of dopes with different salt contents

Membrane	Dope composition (wt%)			Dope viscosity (cp)
	Salt	DMF	PVDF	
A	0	80.0	20	800
B	2.5	78.0	19.5	1050
C	4.8	76.2	19.0	1200
D	7.0	74.4	18.6	2000
E	9.1	72.7	18.2	>2000

membrane morphology. The effect of temperature on crystallization behavior of PVDF during the course of membrane formation was recently reported [8]. It was found that precipitation at high temperatures in a soft bath favored the liquid–liquid demixing process to yield membranes with cellular pores. By contrast, when precipitation was carried out at lower temperatures, crystallization became dominant and the formed membrane consisted of spherical crystallites.

In the present research, the effects of a highly dissociated salt additive, lithium perchlorate, on the physical properties of the precipitated membranes were studied. The gelation phase boundaries were measured for the quaternary system, $LiClO_4$/water/DMF/PVDF at 25 °C. Addition of salt in the casting dope was found to bring a dramatic change to the membrane morphology, as revealed by the SEM imaging. The 'finger-like' voids became longer and widespread and what were the cellular voids are now replaced by irregular macrovoids. This morphological feature is consistent with the measured water permeation and MWCO data. Furthermore, PVDF were found to precipitate into different crystal forms for dopes with and without lithium salt, as revealed by X-ray diffraction spectrums. Differential scanning calorimetric analysis of these membranes indicated the existence of two melting peaks when the scanning rates were ≤ 5 °C/min. The top dense regions of the membranes were examined using low voltage scanning electron microscope (LVSEM) at high magnifications (225 KX) to observe the nano-pores.

2. Experimental

2.1. Material

Poly(vinylidene fluoride), obtained from Elf Ato Chem Inc. (Kynar 740, intrinsic viscosity = 0.982 dl/g, M_n = 298,000 g/mol) was a semicrystalline polymer. *N*,*N*-dimethylformamide (DMF, Baker Analyzed, reagent grade, d = 0.944 g/ml) and water (distilled and deionized) were used, respectively, as the solvent and nonsolvent for the polymer. Lithium perchlorate (Acros, p.a. $\geq$99%) was added to the casting dope to modify the membrane structure. All materials were used as received.

2.2. Phase behavior of the salt/water/DMF/PVDF system

The gelation phase boundaries at 25 °C of the quaternary system, $LiClO_4/H_2O$/DMF/PVDF, were determined by the widely used 'cloud point' method. In brief, a specific amount of PVDF (pre-dried in a vacuum oven at 70 °C) was mixed with DMF and water and then sealed in a Teflon-lined bottle. This mixture was blended at elevated temperature until the polymer was completely dissolved. To this solution was added a known quantity of pre-dried lithium perchlorate (8 h in vacuum at 180 °C). The mixture was blended at ca 110 °C until a visually clear homogeneous solution was obtained. This solution was then placed in a thermostatically controlled bath maintained at 25 °C for a period of 15 days. A gelation point was identified as the composition located between a homogeneous and a precipitated dope.

2.3. Characterization of PVDF gels by DSC and SALS

The crystalline character of the PVDF gels was analyzed using small angle light scattering (SALS) methods [9]. Gel samples were pressed tightly between two glass plates and then placed between two crossed polarizers. A He–Ne laser was used as the light source and the scattering image formed on a ground glass was photographed using a macro lens.

2.4. Membrane preparation and characterization

PVDF membranes were made by the isothermal immersion–precipitation method [1]. Casting dopes were prepared following the procedures described previously. An appropriate amount of the dope was dispersed uniformly on a glass plate and then immersed immediately into water bath to induce polymer precipitation. The dope compositions were listed in Table 1. For dopes containing excess amount of lithium salt (dopes B, C, D, and E) gelation would occur upon standing at 25 °C. These dopes were heated to complete dissolution and subsequently cooled and immersed before precipitation in the bath maintained at 25 °C. The formed membranes were characterized by the methods shown below:

(1) Coarse morphologies of the membranes were observed in cross section, top surface and bottom surface views by SEM at 20 KV (Hitachi, S800).
(2) The nano-scale fine structure of the PVDF crystallites in the membrane was observed by low voltage SEM (Leo, 1530) at high magnifications (e.g. 220 KX, at 0.59 KV).
(3) The crystal structures of the membranes were determined using wide angle X-ray diffraction method (WAXD).
(4) The thermal behavior of PVDF crystallites in the membrane was observed using DSC with different scanning rates over the range 25–230 °C.

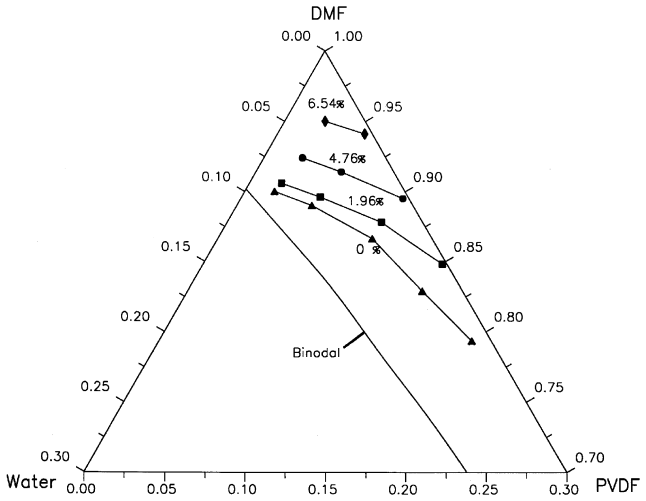

Fig. 1. Phase diagram of the $LiClO_4$/water/DMF/PVDF system at 25 °C. Salt content: 0 wt% (▲); 1.96 wt% (■); 4.76 wt% (●); 6.54 wt% (◆).

(5) FTIR were employed to examine the residual salt content in the formed membrane. A series of films containing known small amounts (25–1000 ppm) of lithium salt were prepared by dry (evaporation of DMF) method. All samples (membranes and films) were re-dissolved in DMF to obtain 2 wt% solutions. Solutions of 10 μl were placed on KBr, which were vacuum dried at 80 °C and then FTIR spectra were taken.

(6) Water permeation rate of the membrane was measured with a dead-end type standard Amicon cell (effective area = 11.9 cm^2) at different transmembrane pressures. The permeation performances of dextran (Aldrich, MW = 70,000) through various membranes at transmembrane pressure of 1.5 atm were measured to see the solute rejection capabilities of the membranes.

(7) Tensile strengths of the membranes were measured by the following procedure. Dried membranes were cut into the standard shape for tensile strength measurements, according to the ASTM (D 638 IV) method. The strengths at break were measured in ambient condition for at least three samples and the average value was reported.

3. Results and discussion

3.1. Phase diagram of $LiClO_4$/water/DMF/PVDF system

Phase diagram of the $LiClO_4$/water/DMF/PVDF system at 25 °C is shown in Fig. 1. For a four-component system, the phase boundaries should occupy a three-dimensional space. Here, for convenience of representation, we have projected the phase boundaries with different salt contents onto the triangle diagram [3]. Since the salt content is small, the error is anticipated to be diminutive. Line '0%' represents the gelation phase boundary with no salt being added (i.e. gelation was induced only by nonsolvent). This phase boundary has been demonstrated previously and is given here for comparison [7]. Upon addition of $LiClO_4$, the gelation line shifts up and the homogeneous solution (one-phase) region becomes smaller. This suggests that in the presence of $LiClO_4$ PVDF becomes less soluble in DMF/water solutions and salting-out phenomenon has taken place [10–13]. Many polymer/solvent systems have been reported to exhibit such behavior. However, there are very few salting-in systems (e.g. methanol is a nonsolvent for PEO but addition of KI results in dissolution of PEO) [10,12]. In order to be salting-in, it is required to have specific interactions among various components in addition to normal electrostatic forces (e.g. PEO–cation interactions in methanol system), which may lead to complex formation in well-defined stoichiometries. For the present research, it appears that ionic interaction between salt/solvent is stronger than that between salt/polymer, leading to PVDF precipitation upon salt addition. The crystalline nature of the precipitated gels was examined using SALS method. Fig. 2 shows the light scattering image of a typical gel (dope 'E' in Table 1) formed at 25 °C. The four-clove pattern clearly indicates that the gel was composed of PVDF crystallites that dispersed uniformly in the dilute phase.

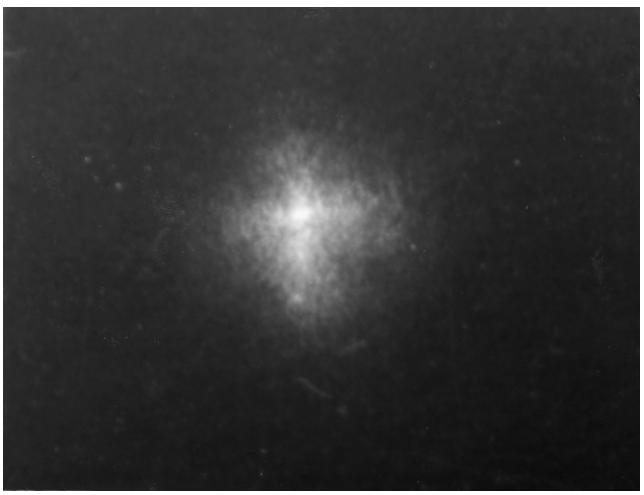

Fig. 2. SALS image of a gel (case 'E' in Table 1). Composition: salt, 9.1 wt%, DMF, 72.7 wt%, PVDF, 18.2 wt%.

3.2. Morphologies of PVDF membranes

In Fig. 3(a)–(e), the cross sections of PVDF membranes prepared by immersing casting dopes with different amounts of $LiClO_4$ into a water bath are presented. All membranes demonstrate the so-called asymmetric morphology being characterized by a thin skin and a porous bulk that comprises large voids extending to the central or even toward the bottom region of the membrane. For the case of adding small amount of $LiClO_4$ in the dope (e.g. 2.5 wt%), the morphology of the formed membrane is similar to that

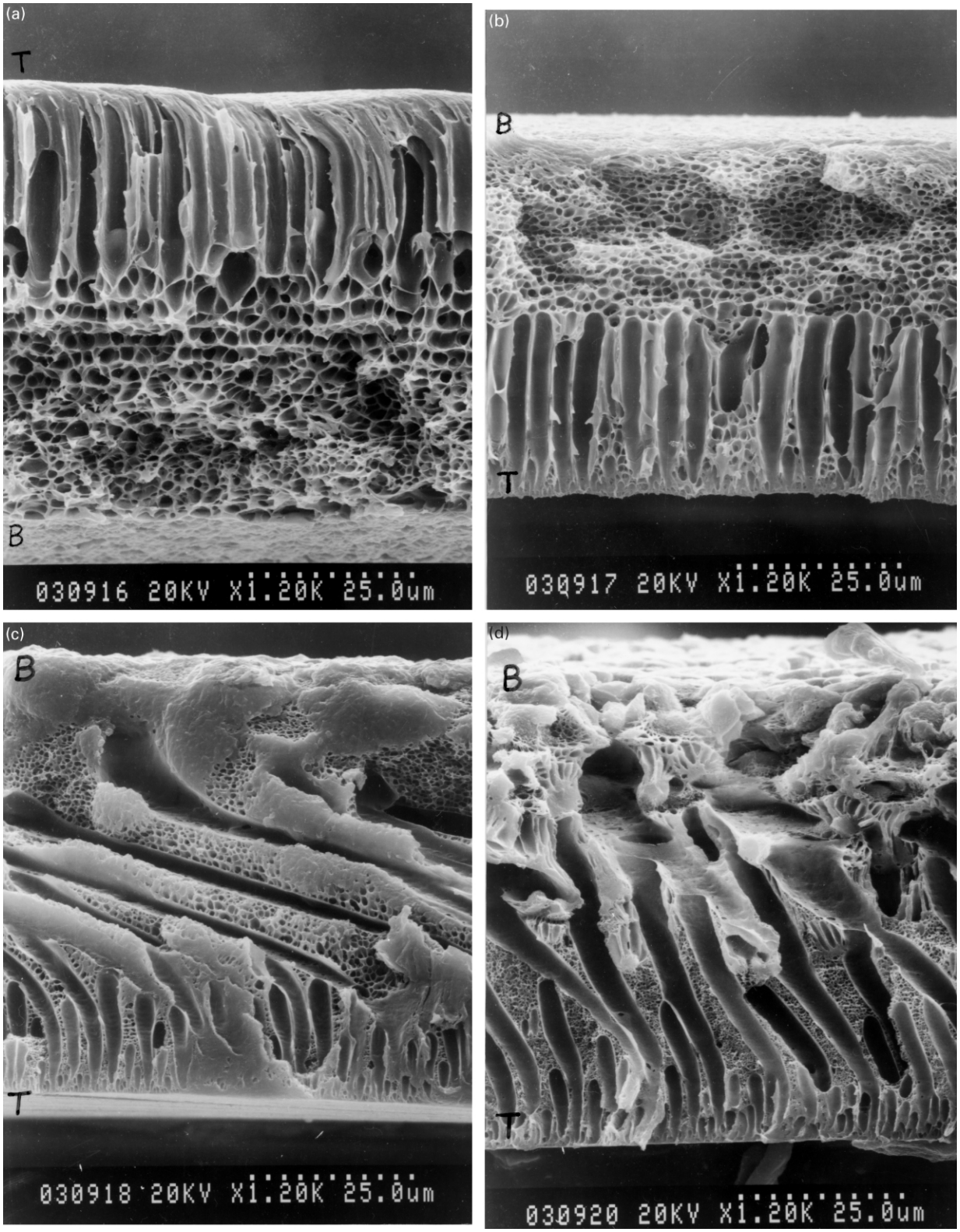

Fig. 3. SEM photomicrographs of the membranes prepared using casting dopes with different salt contents. (a) no salt; (b) 2.5 wt%; (c) 4.8 wt%; (d) 7 wt%; (e) 9.1 wt%. T, top surface; B, bottom surface.

prepared by a salt-free dope. The upper half of the cross section is composed of parallel finger-like voids, whereas the lower half is composed of small independent cellular pores that are enclosed in a polymer matrix. These morphological features are typically observed in amorphous membranes (e.g. PMMA, polysulfone, etc.) and are known to be derived from liquid–liquid phase demixing process [1,14,15]. Although this kind of morphology suggests a

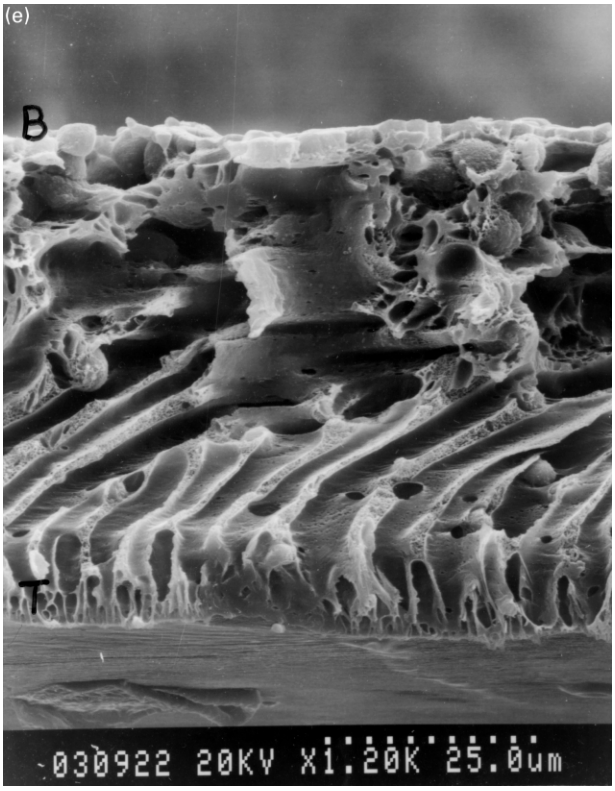

Fig. 3 (*continued*)

liquid–liquid demixing dominant precipitation situation, crystallization indeed occurred during the late stage of the precipitation process. While liquid–liquid demixing has completely established the bulk porous structure, crystallization could take effect only on the gel phase that surrounds the cellular pores [7,8,16,17]. Evidence of crystallization during precipitation will be shown later via DSC analysis and X-ray diffraction of the membranes.

As more lithium salt was added to the casting dope, the formed membranes became more porous. As shown in Fig. 3(c) for the case of adding 4.8% salt in the dope, the finger-like voids here are much larger and they extend bending toward the bottom region. In Fig. 3(c), some small cellular pores between macrovoids can still be observed over the cross section. However, when the salt content of the dope was larger than ca 7 wt%, the formed membranes demonstrated an uncommon structure (Fig. 3(d) and (e)); what were the cellular regions are now occupied by irregular large voids and the polymer near the bottom aggregated into large blocks of identities (ca 5 μm). The reasons for the formation of the large voids in membranes prepared by immersion–precipitation method has been extensively studied in the literature [18–23]. A number of mechanisms have been proposed, e.g. surface breakage due to shrinkage stress proposed by Strathmann, liquid–liquid demixing and diffusional growth of cellular pores by Reuvers et al., osmosis effect during growth of cellular pores by Koros et al., instability caused by perturbation of the interface in steep concentration profile by Ray et al. However, no solid conclusion has been reached yet. For the current system, the concept of osmosis effect offers an explanation. As a liquid micell is formed from liquid–liquid demixing, it will dissolve some lithium salt in it (apparently, upon phase separation, salt tends to go into the liquid micell rather than stay in the concentrated gel phase that contains a large amount of polymer). Since the cell wall may act somewhat like a skin layer, a large osmosis force was created between the micell and its surrounding gel phase. This force drove DMF/water into the micell, which further accelerated the growth of macrovoids.

The crystallization-associated morphology is most evident in the region near the bottom surface (large blocks of identities), particularly, for membranes prepared using dopes with a high salt content (e.g. larger than 7%). This is because high salt content dopes are in meta-stable states that are highly supersaturated with respect to PVDF crystallization (Fig. 1) and there may exist considerable amount of pre-nucleation embryos in these dopes [7,8,16,17]. The viscosity data of various dopes, as shown in Table 1, support this point. As can be seen that the viscosities increase dramatically from dope 'C' (4.8 wt% salt) to dope 'D' (7 wt% salt). Moreover, it was also observed that dopes D and E gelled soon after viscosity measurements, which suggested that the sharp increase in dope viscosity between dopes C and D was caused by polymer crystallization. The other factor that favors crystallization to take place near the bottom surface is that

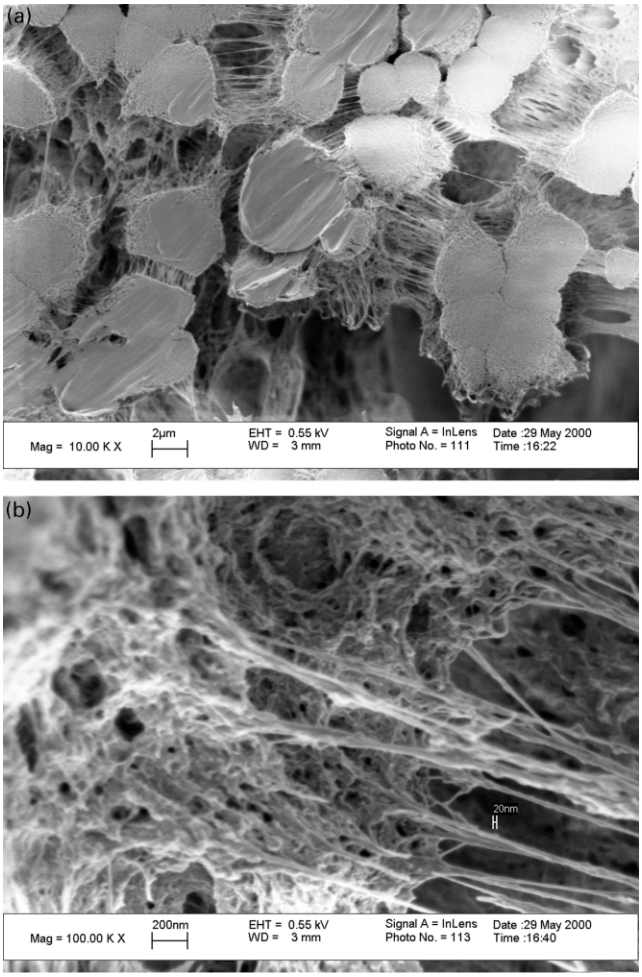

Fig. 4. SEM photomicrographs of the bottom surface of membrane E. Magnification: (a) 10 KX; (b) 100 KX.

during the precipitation process, it takes a considerably long time for nonsolvent to reach the bottom region to induce liquid–liquid demixing [7]. Hence, crystallization can take place exclusively in this region. As an example, Fig. 4(a) and (b) illustrated the bottom surface (the surface facing the glass plate) of the membrane prepared by the dope containing 9.1 wt% salt (membrane 'E' in Table 2). The cellular pores derived typically from liquid–liquid demixing process are not observed here and the PVDF precipitated into groups of truncated globule-like particles (ca 5 μm). The boundaries between particles carry a linear feature and sometimes the particles are interconnected by sets of fibrils. Some particle surfaces appear flattened as a result of their growth against the glass plate during precipitation. Apparently, crystallization has dominated the precipitation process in the bottom region of this membrane. The nano-scale fine structure of the particles was observed under high magnifications. To avoid the artifacts caused by metal coating of the sample (a common practice to enhance electrical conductivity for SEM imaging), uncoated membranes were employed. This was made possible by applying very low acceleration voltage (typically, 0.6 KV) during imaging such that surface charging and damaging caused by impinging electrons were minimal. Fig. 4(a) shows the surface structure of a truncated globular particle and fibrils that connect this particle with others. Quite interestingly, a porous surface is revealed at this high magnification and some nano-pores (10 nm) are evident. The crystallites here are twig-like with considerable branching; the width of a twig falls largely over the range 10–20 nm. This is comparable with the interlamellar distance of PVDF crystallites in various types of samples (nonporous film, fiber, porous membrane) reported in the literature, as measured by SAXS, TEM, and AFM methods [8,24–26]. The fine structures of the fibrillar material, which tie the globular particles, are also clearly presented in Fig. 4(b). The thickness of a single string is less than 15 nm. Bundles of strings branch out at the ends, where they join the globular particle at different points.

The structure of the top surface (i.e. skin) of the above membrane is shown in Fig. 5. It can be seen that this surface contains many small pores, in contrast to normal understanding that the skin is nonporous. As conventional SEM imaging uses samples with a layer of metal (ca 20–50 nm) coating on it, it is possible that small nano-pores are filled up and hence not visible. Similar to our observation, Jian et al. used transmission electron microscope (TEM) to identify small pores (30 nm) near the top surface region of an asymmetric PVDF membrane prepared by phase inversion from water/DMAC/acetone/PVDF system [27]. At the magnification of 225 KX (Fig. 5(b)), one can observe nonpenetrating nano-pores (<20 nm) on the top surface. These pores can contribute (although limitedly) to the permeation fluxes. As these pores are shallow, they were formed in the gel layer just underneath the membrane-bath interface. As the gel was stiff due to high polymer concentration, further growth of the pores is impossible [7,16].

Table 2
Properties of membranes prepared using dopes of different salt contents

Membrane	Water flux ($\Delta P = 1.5$ atm) (g/min cm^2)	UF permeation[a] ($\Delta P = 1.5$ atm) (%)	Crystal form of PVDF	Tensile strength (Kgf)
A	0.011	94.5	α	0.432
B	0.016	91.7	β	0.393
C	0.045	87.6	β	0.237
D	0.240	36.4	β	0.122
E	0.334	24.8	β	0.103

[a] The percentage of dextran (MW = 70,000) permeating through the membrane.

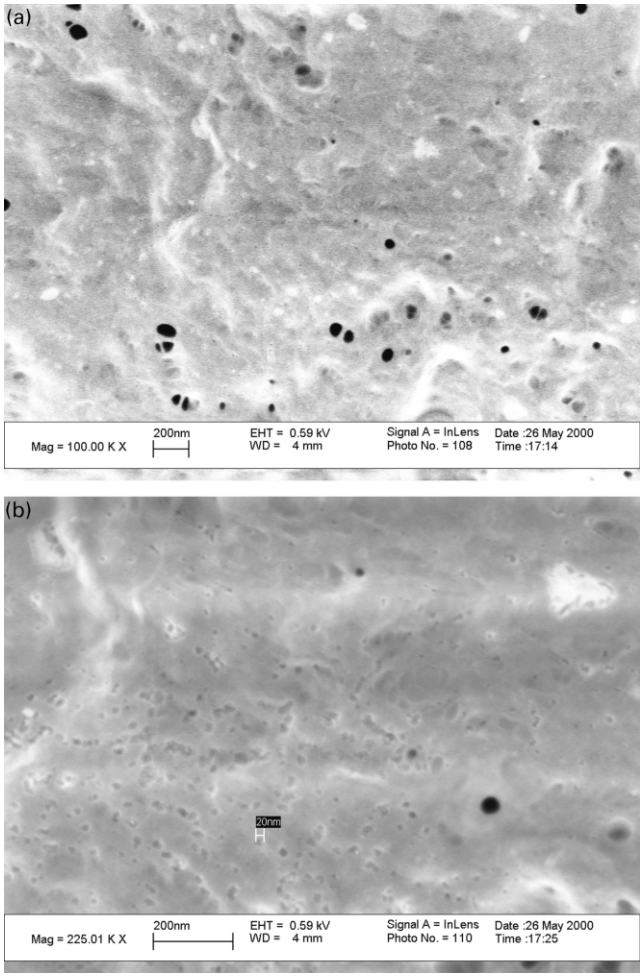

Fig. 5. SEM photomicrographs of the top surface of membrane E. Magnification: (a) 100 KX; (b) 225 KX.

3.3. Salt content in the PVDF membrane

The salt content in the formed membrane was analyzed using FTIR. In Fig. 6, FTIR spectrum of the membrane prepared by immersing a dope containing 9.1 wt% lithium salt in water is shown together with PVDF films (nonporous, transparent) that contain known amounts (25–1000 ppm) of lithium salt. These films were prepared by the dry (solvent evaporation) method [1]. For these nonporous PVDF films, spectra 'A', 'B', and 'C' indicate that the intensity of the absorption peaks near 1632 nm (characteristic of lithium perchlorate) decrease with decreasing salt content in the film. And when the salt content is less than 25 ppm (curve 'C'), this peak becomes insignificant. The absorption spectrum of the PVDF membrane is shown in curve 'D'. It appears that there is no observable peak near 1632 nm. In other words, its salt content is less than 25 ppm. Therefore, it can be concluded that lithium salt in the original casting dope (9.1 wt%) has been leached out nearly completely during the course of the precipitation process. This is consistent with the fact that lithium perchlorate favors the company of water/DMF solutions rather than PVDF and

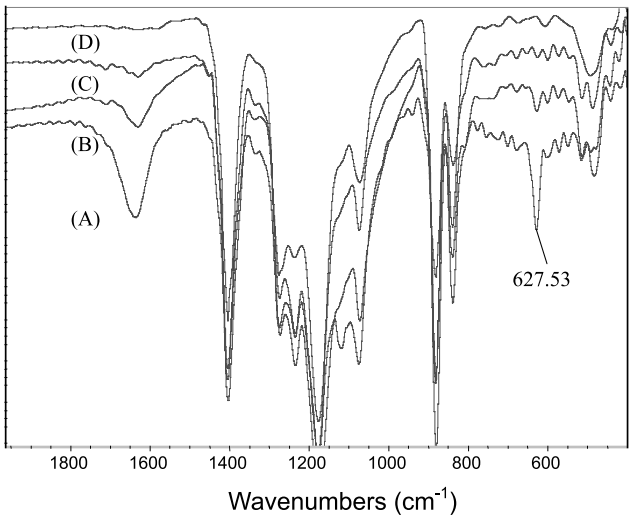

Fig. 6. FTIR spectrums of PVDF membrane and salt-containing films. (a) 1000 ppm $LiClO_4$ film; (b) 100 ppm $LiClO_4$ film; (c) 25 ppm $LiClO_4$ film; (d) membrane E.

that during crystallization PVDF tends to reject impurities into its surrounding liquid phase. The salt-out effect shown earlier in the phase diagram also supported this observation. In contrast to the present result, Kim has reported a situation, where zinc chloride was found to enhance dissolution of polysulfone in NMP solutions by the mechanism of complex formation [3]. And because of this specific interaction, the membranes prepared from the latter dopes were reported to contain substantial amount of zinc chloride.

3.4. Crystal structure and thermal behavior of the PVDF membrane

All of the membranes shown in Fig. 3 are inherently crystalline, although their bulk morphologies may exhibit features (e.g. cellular pores) that are frequently observed in amorphous membranes. In addition to the membrane morphology, lithium salt also exerted marked influence on the PVDF crystal structure in the membrane. This is evident in the wide-angle X-ray diffraction spectra shown in Fig. 7. Curves A, B, and C represent membranes 'A' (dope containing no salt), 'B' (dope containing 2.5 wt% salt), and 'E' (dope containing 9.1 wt% salt), respectively. It appears that two types of crystal forms exist in these membranes. Compared with the crystallographic data in the literature [28,29], one can conclude: (1) when the dope is free of lithium perchlorate, the membrane precipitated into α type structure (i.e. type II), wherein PVDF was orientated in an orthorhombic crystal unit cell. The three characteristic peaks at 18.46, 20.24, and 26.62° in spectrum A correspond to the reflections at (200), (110), and (201) planes, respectively. (2) With addition of lithium salt (≥2.5 wt%) in the dopes, the membranes exhibited largely β (i.e. type I)

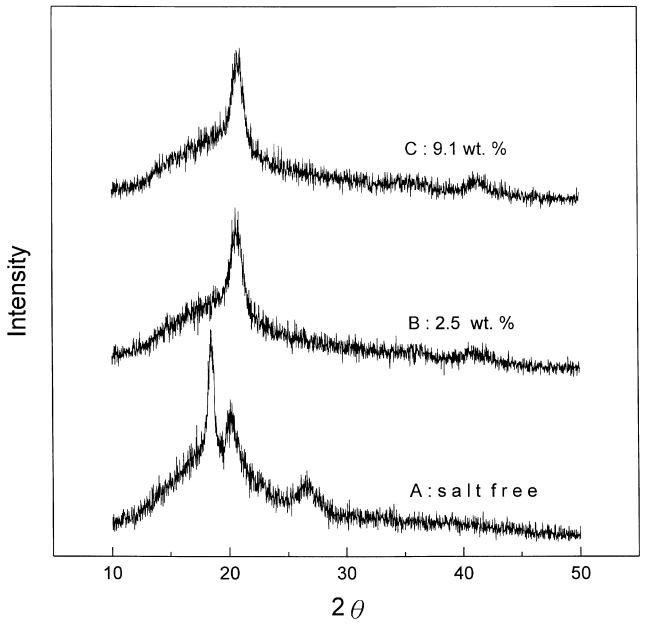

Fig. 7. X-ray diffraction patterns of PVDF membranes prepared using casting dopes with different salt contents. (a) salt-free; (b) 2.5 wt%; (c) 9.1 wt%.

crystal structure. The broad peak near 20.68° represented contributions from the reflections at (110) plane of β form.

The PVDF membranes, formed by precipitation from concentrated solutions, sometimes contain crystallites that are small and imperfect, as revealed by the DSC analysis [30]. In Fig. 8(a) and (b), the thermograms at different heating rates (1–40 °C/min) of a typical membrane (membrane E) are shown. It can be seen that the melting peak temperature changes with the scanning rate and that there exists a second peak when the scanning rate is ≤5 °C/min. The first broad peak at lower temperature can be attributed to the melting of the smaller less perfect crystals. While they melt, perfection of the metastable crystals is also occurring. This leads to the formation of crystals that may contain thicker lamellae, which subsequently melt at the second higher peak temperature. When the heating rate is higher than 10 °C/min, only one peak is observed and when the heating rate reached 40 °C/min, superheating takes effect and an unreasonably high peak temperature results. Membranes with PVDF crystallites in different crystal forms (e.g. α-, β-form) also exhibit different melting temperatures, as is indicated in Fig. 9. The open and the filled symbols represent, respectively, membranes in α (membrane A) and β (membrane E) crystal forms. It appears that the β form has a higher melting point than the α form crystal, although the latter has been identified to be the more stable form [30]. Prest and Luca have studied the melting behavior of melt-crystallized PVDF samples [31]. From annealing experiments, they concluded that the level of crystal perfection (less defects) rather than the stability of crystal structure determines the melting temperature.

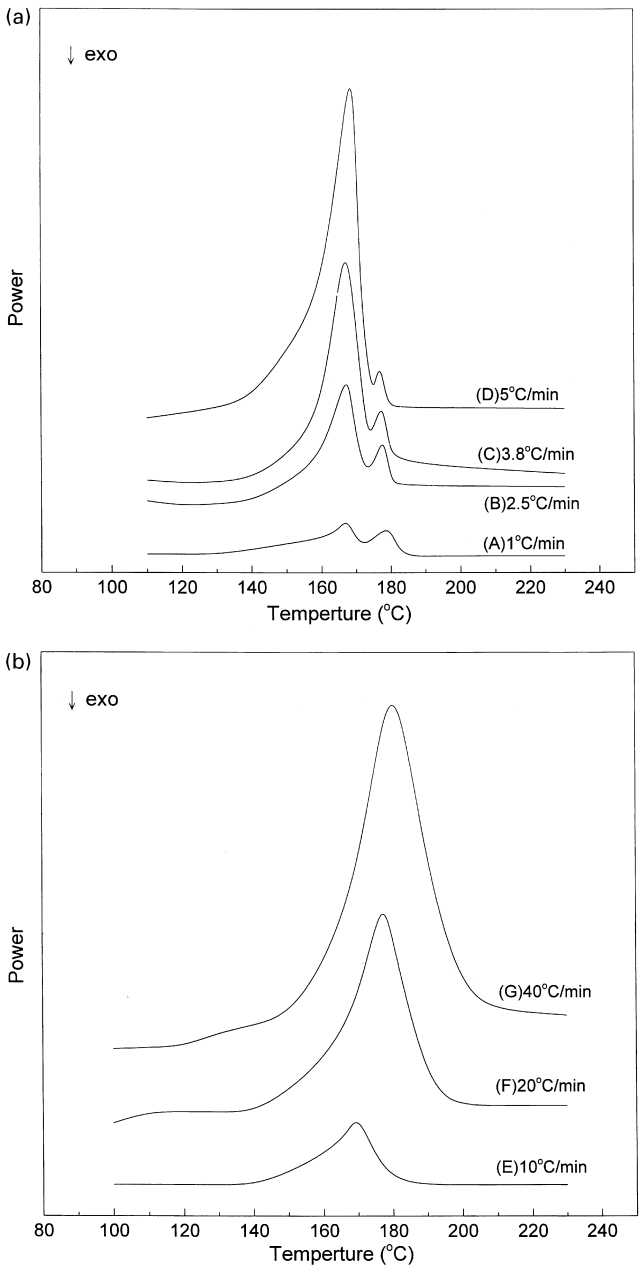

Fig. 8. DSC thermograms of membrane E at various scanning rates. (a) rates = 1, 2.5, 3.8, 5 °C/min, respectively; (b) rates = 10, 20, 40 °C/min, respectively.

3.5. Permeation performance and tensile strength

For the asymmetric PVDF membranes prepared in this work, ultrafiltration applications are expected to be operative. The porosity of the membranes increased with increasing salt content in the dope, as suggested by the SEM shown previously. This effect is also evident from the water flux data presented in Fig. 10, measured by a standard Amicon cell over the transmembrane pressure range of 0.5–3.5 atm (for ordinary microfiltration and ultrafiltration applications). As can be seen, the water fluxes of the tested membranes decrease following the order:

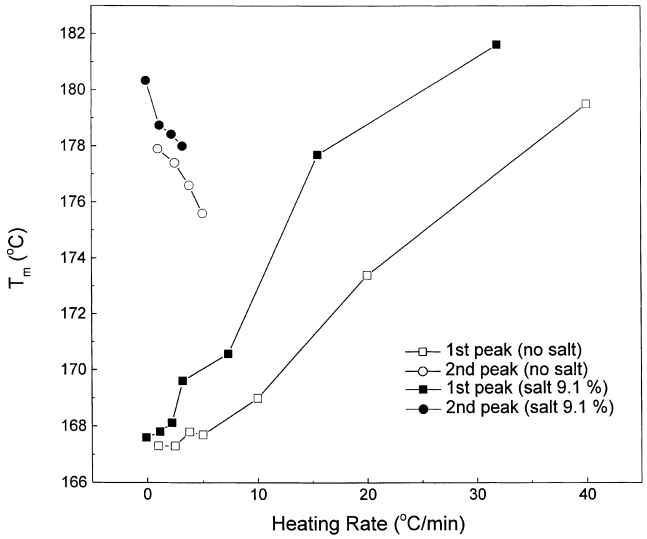

Fig. 9. Melting peak temperatures of PVDF membranes as a function of heating rate. ■, ●: membrane E, β type crystals; □, ○: membrane A, α type crystals.

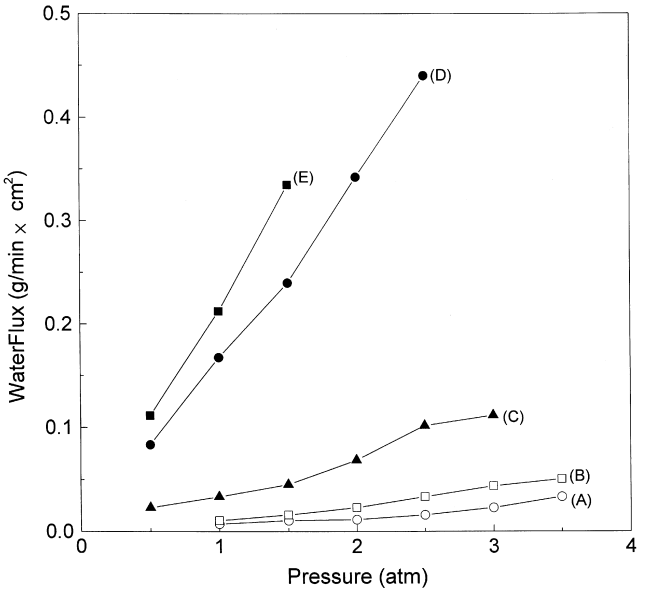

Fig. 10. Water permeation fluxes of PVDF membranes prepared by dopes with different salt contents. (a) salt-free; (b) 2.5 wt%; (c) 4.8 wt%; (d) 7 wt%; (e) 9.1 wt%.

A < B < C < D < E, consistent with the fact that the skin of the membrane became less tight and the bulk became more porous when salt was added in the dope. The permeation performances of dextran (MW = 70,000) through the membranes are shown in Table 2. It can be seen that both of the membranes A and B reject more than 90% of the dextran in the feed. By contrast, membranes D and E have a poor rejection. And there is a large gap for rejection performance between membranes C and D. This is consistent with the water flux, the dope viscosity, and the membrane structure shown earlier. The tensile strengths of the membranes are shown in Table 2. Obviously, these membranes have proper strengths to sustain ultrafiltration operations. It is interesting to find that the tensile strengths decrease with increasing salt contents in the dope and that there is a sharp change between membranes C and D. This again reflects the fact that the membranes become more porous with increasing salt contents in the dopes and that there is large change in structure between membranes C and D.

4. Conclusion

The salt additive, lithium perchlorate, affected significantly the gelation phase behavior of PVDF in water/DMF solutions as well as the properties of the PVDF membranes made by the immersion–precipitation process. The effects are summarized below:

(1) The crystallization-induced gelation boundaries shifted up with increasing salt contents in the dopes. (2) With addition of salt in the dope, the formed membrane became more porous. When the salt content of the dope exceeded ca 7 wt%, very large macrovoids were formed, which extended to the bottom region of the membrane. And the cellular region was replaced by large voids and large blocks of crystal identities. (3) Lithium perchlorate did not retain in the membrane even with a casting dope containing 9.1 wt% salt. (4) PVDF precipitated from salt-containing dopes into α-type crystals in the formed membrane. By contrast, for salt-free dopes, the precipitated membrane consists α-type crystals. (5) The skin region of the membrane prepared from high salt content dopes contains very small pores (some 10th nm), which is related to its high permeation fluxes and low solute rejections.

Acknowledgements

This research was supported by the National Council of Taiwan, ROC (NSC 87-2216-E-032-001).

References

[1] Kesting RE. Synthetic polymeric membranes. New York: Wiley; 1985.
[2] Bottino A, Capannelli G, Munari S, Turturro A. Dealination 1988;68:167.
[3] Kim SR, Lee KH, Jhon MS. J Membr Sci 1996;119:59.
[4] Kraus MA, Nemas M, Frommer MA. J Appl Polym Sci 1979;23:445.
[5] Wang D, Li K, Teo WK. J Membr Sci 2000;178:13.
[6] Lai JY, Huang SJ, Chen SH. J Membr Sci 1992;74:71.
[7] Cheng LP, Lin DJ, Shih CH, Dwan AW, Gryte CC. J Polym Sci B: Polym Phys 1999;37:2079.
[8] Cheng LP. Macromolecules 1999;32:6668.
[9] Meeten GH. Optical properties of polymers. London: Elsevier; 1986.
[10] Gray FM. Solid polymer electrolytes. New York: VCH Publishers; 1991.
[11] Bailey FE, Callard RW. J Appl Polym Sci 1959;1:373.

[12] Lundberg RD, Bailey FE, Callard RW. J Polym Sci 1966;A1(4):1563.
[13] Quina F, Sepuveda L, Sartori R, Abuin EB, Pino CG, Lissi EA. Macromolecules 1986;19:994.
[14] Mulder M. Basic principles of membrane technology. Dordrecht: Kluwer; 1991.
[15] Cheng LP, Shaw HY. J Polym Sci B: Polym Phys 2000;38:747.
[16] Young TH, Lin DJ, Gau JJ, Chuang WY, Cheng LP. Polymer 1999; 40:5011.
[17] Cheng LP, Dwan AW, Gryte CC. J Polym Sci B: Polym Phys 1995; 33:211.
[18] Strathmann H. In: Lloyd DR, editor. Material science of synthetic membrane. ACS Symposium Series, Washington, DC: American Chemical Society; 1985.
[19] Smolders CA, Reuver AJ, Boom RM, Wienk IM. J Membr Sci 1992; 73:259.
[20] McKelvey SA, Koros WL. J Membr Sci 1996;112:29.
[21] Ray RJ, Krantz WB, Sani RL. J Membr Sci 1985;23:155.
[22] Lai JY, Lin FC, Wu TT, Wang DM. J Membr Sci 1999;155:31.
[23] Termonia Y. J Membr Sci 1995;104:173.
[24] Nakagawa K, Ishida Y. J Polym Sci, Polym Phys 1973;11:2153.
[25] Cakmak M, Teitge A, Zachmann HG, White JL. J Polym Sci B: Polym Phys 1993;31:371.
[26] Wunderlich B, Macromolecular physics, vol. 1. New York: Academic Press; 1973.
[27] Jian K, Pintauro PN, Ponangi R. J Membr Sci 1996;117:117.
[28] Lovinger AJ. In: Bassett DC, editor. Developments in crystalline polymers-1. Barking: Applied Science Publisher; 1988.
[29] Davis GT, McKinney JE, Broadhurst MG, Roth SC. J Appl Phys 1978;49:4998.
[30] Wunderlich B, Macromolecular physics, vol. 3. New York: Academic Press; 1980.
[31] Prest WM, Luca DJ. J Appl Phys 1975;46:4136.